Article

Unveiling the Magnetic and Structural Properties of (X₂YZ; X = Co and Ni, Y = Fe and Mn, and Z = Si) Full-Heusler Alloy Microwires with Fixed Geometrical Parameters

Mohamed Salaheldeen [1,2,3,4,*] , Valentina Zhukova [1,2,4] , Mihail Ipatov [1,2] and Arcady Zhukov [1,2,4,5,*]

1   Department of Polymers and Advanced, Chemistry Faculty, University of Basque Country, UPV/EHU, 20018 San Sebastián, Spain; valentina.zhukova@ehu.es (V.Z.); mihail.ipatov@ehu.es (M.I.)
2   Department of Applied Physcs, Faculty of Engineering of Gipuzkoa, EIG, University of Basque Country, UPV/EHU, 20018 San Sebastián, Spain
3   Physics Department, Faculty of Science, Sohag University, Sohag 82524, Egypt
4   EHU Quantum Center, University of the Basque Country, UPV/EHU, 20018 San Sebastián, Spain
5   IKERBASQUE, Basque Foundation for Science, 48011 Bilbao, Spain
*   Correspondence: mohamed.salaheldeenmohamed@ehu.eus (M.S.); arkadi.joukov@ehu.es (A.Z.)

Abstract: We studied Ni₂FeSi-, Co₂FeSi-, and Co₂MnSi-based full-Heusler alloy glass-coated microwires with the same geometric parameters, i.e., fixed nucleus and total diameters, prepared using the Taylor–Ulitovsky method. The fabrication of X₂YZ (X = Co and Ni, Y = Fe and Mn, and Z = Si)-based glass-coated microwires with fixed geometric parameters is quite challenging due to the different sample preparation conditions. The XRD analysis showed a nanocrystalline microstructure for all the samples. The space groups Fm3⁻m (FCC) and Im3⁻m (BCC) with disordered B2 and A2 types are observed for Ni₂FeSi and Co₂FeSi, respectively. Meanwhile, a well-defined, ordered L2₁ type was observed for Co₂MnSi GCMWs. The change in the positions of Ni, Co and Mn, Fe in X₂YSi resulted in a variation in the lattice cell parameters and average grain size of the sample. The room-temperature magnetic behavior showed a dramatic change depending on the chemical composition, where Ni₂FeSi MWs showed the highest coercivity (H_c) compared to Co₂FeSi and Co₂MnSi MWs. The H_c value of Ni₂FeSi MWs was 16 times higher than that of Co₂MnSi MWs and 3 times higher than that of Co₂FeSi MWs. Meanwhile, the highest reduced remanence was reported for Co₂FeSi MWs (Mr = 0.92), being about 0.82 and 0.22 for Ni₂FeSi and Co₂MnSi MWs, respectively. From the analysis of the temperature dependence of the magnetic properties (H_c and M_r) of X₂YZ MWs, we deduced that the H_c showed a stable tendency for Co₂MnSi and Co₂FeSi MWs. Meanwhile, two flipped points were observed for Ni₂FeSi MWs, where the behavior of H_c changed with temperature. For M_r, a monotonic increase on decreasing the temperature was observed for Co₂FeSi and Ni₂FeSi MWs, and it remained roughly stable for Co₂MnSi MWs. The thermomagnetic curves at low magnetic field showed irreversible magnetic behavior for Co₂MnSi and Co₂FeSi MWs and regular ferromagnetic behavior for Ni₂FeSi MWs. The current result illustrates the ability to tailor the structure and magnetic behavior of X₂YZ MWs at fixed geometric parameters. Additionally, a different behavior was revealed in X₂YZ MWs depending on the degree of ordering and element distribution. The tunability of the magnetic properties of X₂YZ MWs makes them suitable for sensing applications.

Keywords: full-Heusler alloys; glass-coated microwires; magnetic behavior; sensing applications

1. Introduction

Heusler alloys, characterized by their typical X₂YZ (full-Heusler) or XYZ (half-Heusler) compositions, represent a category of multifunctional materials [1–5]. Extensive research has been devoted to investigating the properties of Heusler alloys due to their diverse range of properties, such as the shape memory effect, substantial magnetic-field-induced strain (MFIS),

half-metallic behavior, giant magnetocaloric effect (MCE), and exchange bias [3–9]. Heusler alloys are suitable for a variety of applications owing to their characteristics, especially in the fields of magnetic cooling, actuators, and energy harvesting [10–12]. Numerous bulk Heusler alloys have been successfully synthesized over time, and their structural and physical characteristics have been extensively studied.

Arc melting, followed by additional thermal treatment, is the main technique used to produce Heusler alloys [2,3,10]. This method makes it possible to produce Heusler alloys in bulk form. However, miniaturization has been investigated as an alternative approach to improve the aforementioned characteristics of Heusler alloys [10]. The performance of Heusler alloys can be improved noticeably by minimizing the dimensions of the alloys. For instance, in the context of magnetic cooling applications, the surface-to-volume ratio can be enhanced to significantly improve the heat-exchange rate by using low-dimensional Heusler alloys.

In recent years, growing attention has been paid to the synthesis and investigation of different families of Heusler alloys with reduced dimensions, such as thin micro/nanowires, ribbons, nanoparticles, and thin films [13–15]. However, the inherent brittleness of Heusler compounds, including Co-, Fe-, and Ni-based full-Heusler alloys, poses a challenge for their fabrication using conventional metallurgical techniques. Consequently, significant efforts have been directed toward the development of novel fabrication methods for producing Heusler alloys in different physical forms for a specified application. These endeavors aim to overcome the limitations imposed by brittleness and explore the potential of low-dimensional Heusler alloys. Additionally, the preparation of composites incorporating Heusler alloys has emerged as a promising approach to address the aforementioned brittleness issue, becoming a topic of considerable interest in the development of this family of functional materials [3,10].

Rapid melt quenching has been recognized by scientists since the 1960s as a commonly used method to produe innovative materials with a variety of morphological characteristics, including amorphous or crystalline (micro/nanocrystalline) structures, as well as metastable phases with reduced dimensions [16,17]. Using this technology, it is possible to obtain alloys with specified chemical compositions using rapid solidification, obtaining materials with more effective mechanical, magnetic, and corrosion properties [18–20]. Rapid melt quenching techniques have been developed to produce ribbons, wires, flakes, microwires, composite microwires, and other materials. The chosen alloy's phase diagram, the quenching conditions, and the geometry of the prepared materials are only a few of the specific fabrication features that are critical in determining the final structure of the materials that are produced.

As previously mentioned, crystalline rapidly quenched materials generally exhibit inferior mechanical properties compared to their amorphous counterparts [20]. However, other properties relevant to various applications, such as enhanced corrosion resistance and biocompatibility, are desirable [21]. Furthermore, the miniaturization of rapidly quenched materials has emerged as a challenge for numerous applications. Consequently, the development of preparation methods capable of meeting these expectations has garnered significant attention in recent years.

One particularly promising technology aiming at the miniaturization of rapidly quenched materials while simultaneously improving magnetic, corrosion, and mechanical properties is the Taylor–Ulitovsky technique [22–24]. This technique enables the fabrication of thin metallic microwires (typically ranging from 0.02 to 100 μm in diameter) coated with a layer of glass [23–30]. The resulting thin glass-coated microwires, with either amorphous or nanocrystalline structures, can exhibit excellent magnetic softness. Additionally, the thin glass coating imparts new functionalities, including enhanced mechanical and corrosion properties, favorable adhesion to polymeric matrices, and biocompatibility [31–33]. In this regard, a few successful endeavors have been made using either the in-rotating-water technique to fabricate wires [34] or the Taylor–Ulitovsky technique to prepare glass-coated microwires from Heusler alloys [35–41]. These advances represent significant progress in

the preparation of Heusler alloys in low-dimensional forms and have opened up opportunities for further exploration.

One of the peculiarities of the Taylor–Ulitovsky technique is that it allows the preparation of metallic microwires coated with insulating glass by simultaneous rapid solidification from the melt. This manufacturing method is intrinsically linked with internal stresses arising mostly due to the difference in the thermal expansion coefficients of the glass coating and the metallic alloy [18,42–44]. The magnitude of the internal stresses, σ_i, correlates with the ratio, ρ, between the metallic nucleus diameter, d_{metal}, and the total diameter, D_{total}. In this way, σ_i can be modified by changing the ρ–ratio [42,44].

In this study, we present an endeavor to produce a set of glass-coated microwires based on the X_2YZ composition. These microwires were designed with fixed geometric parameters and a high Curie temperature exceeding 900 K. The objective was to examine the impact of the uniform internal stress induced by the glass layer coating on the magnetic and structural behavior of the samples, utilizing the Taylor–Ulitovsky process. The selection of this fabrication method was driven by the intriguing magneto-structural characteristics exhibited by glass-coated microwires derived from Heusler alloys, along with the advantageous functional properties associated with such microwires. We chose a series of Heusler alloys, i.e., Ni_2FeSi, Co_2FeSi, and Co_2MnSi, with a high Curie temperature, which have a significant contribution in advanced spintronic applications due to their unique physical, electronic, and magnetic properties [2,12,14,17]. A strong dependence of the magnetic and structural properties of X_2YZ-based glass-coated microwires on fixed geometric parameters was observed, and this reveals the sensitivity of the internal stress to the microstructure ordering and the chemical composition of the metallic nuclei of X_2YZ-based glass-coated microwires.

2. Materials and Methods

The experimental conditions for the preparation Ni_2FeSi, Co_2FeSi, and Co_2MnSi in bulk and glass-coated microwires are described in detail in our previous works [12,14,17]. The key point and objective of the current study is to fabricate the samples with fixed geometric parameters to investigate the effect of the internal stresses originated by the covering glass layer on the magnetic properties and microstructure in different series of X_2YZ-based full-Heusler glass-coated microwires.

The following procedures were used to prepare Ni_2FeSi, Co_2FeSi, and Co_2MnSi alloys by arc melting. The precursor elements for the Ni_2FeSi, Co_2FeSi, and Co_2MnSi alloys were weighed to fit with the nominal ratio (X)2:(Y)1:(Z)1) and deposited in a graphite crucible, containing Ni (99.99%), Co (99.99%), Fe (99.9%), Mn (99.99%), and Si (99.99%). The ingots of Ni_2FeSi, Co_2FeSi, and Co_2MnSi alloys (ingot) were created by combining the ingredients. For all alloys, the melting process was repeated five times to make the alloys homogenous. The chemical compositions and the nominal ratio of the X_2YZ alloys were tested before proceeding to the glass-covering process. By using the Taylor–Ulitovsky technique, we can obtain a wide range of Heusler-based glass-coated microwires with proper dimensions and length depending on the application and the purpose of the investigations [22,26,37,41–47]. Controlling the casting process rate of the melting ingot, i.e., Ni_2FeSi, Co_2FeSi, and Co_2MnSi, enabled us to obtain glass-coated microwires with a fixed nuclei diameter and well-controlled thickness of the covering glass layer. Thus, fixed geometric parameters were easily obtained in the current alloys. After preparation of the Ni_2FeSi, Co_2FeSi, and Co_2MnSi MWs, we estimated the geometrical parameters d_{metal} (μm), D_{total} (μm), and the aspect ratio ($\rho = d_{metal}/D_{total}$) by using an optical microscope and Scanning Electron Microscopy (SEM) and Energy Dispersive X-ray (EDX) (JEOL-6610LV, JEOL Ltd., Tokyo, Japan) to determine the geometric parameters of the Ni_2FeSi, Co_2FeSi, and Co_2MnSi MW samples and their related nominal chemical compositions (see Table 1). After confirming the nominal ratio and the chemical compositions of the Ni_2FeSi, Co_2FeSi, and Co_2MnSi MWs, microstructure analysis was performed at room temperature by using X-ray diffraction (XRD) (D8 Advance, Bruker AXS GmbH, Karlsruhe, Germany). The

magnetic characterizations were performed as follows: First, we measured the hysteresis (M-H) loops at room temperature by applying a magnetic field parallel and perpendicular to the metallic nuclei axis of the Ni_2FeSi, Co_2FeSi, and Co_2MnSi MW samples to check the magnetic anisotropy and confirm the easy axis of the magnetization. Then, we checked the magnetic behavior of the samples in a wide range of temperature (5–400 K) by measuring the M-H loops parallel to the wire's axis, i.e., the easy magnetization axis. Finally, we analyzed the thermal magnetization curves, i.e., the field cooling (FC) and field heating (FH) magnetizations curves at applied low external magnetic field, to check the irreversibility behavior or magnetic phase transition in the Ni_2FeSi, Co_2FeSi, and Co_2MnSi MWs. All magnetization curves were measured using a PPMS (Physical Property Magnetic System, Quantum Design Inc., San Diego, CA, USA) vibrating-sample magnetometer.

Table 1. The geometrical parameters d_{metal} (µm), D_{total} (µm), nominal ratio, and average (Av.) of atomic percentage of Ni, Co, Fe, Mn, and Si elemental composition in as-prepared Ni_2FeSi, Co_2FeSi, and Co_2MnSi glass-coated microwires.

Sample	d_{metal} (µm)	D_{total} (µm)	Chemical Composition	Nominal Ratio
Ni_2FeSi	10.79 ± 0.1	21.02 ± 0.1	$Ni_{51}Fe_{23}Si_{26}$	2:1:1
Co_2FeSi	10.35 ± 0.1	20.88 ± 0.1	$Co_{48}Fe_{25}Si_{31}$	2:1:1
Co_2MnSi	9.83 ± 0.1	19.94 ± 0.1	$Co_{46}Mn_{24}Si_{30}$	2:1:1

3. Results

3.1. Chemical, Nominal Composition, and Microstructure Analysis

As mentioned in the previous section, the morphological and main geometrical parameters were evaluated using an optical microscope and SEM. Figure 1 illustrates the SEM images of the Ni_2FeSi, Co_2FeSi, and Co_2MnSi MWs with fixed geometrical parameters. Table 1 shows the estimation of the metallic nucleus, d_{metal}, and the total diameters, D_{total}, of the Ni_2FeSi, Co_2FeSi, and Co_2MnSi MWs. By calculating d_{metal} (µm) and D_{total} (µm), we can easily confirm that the samples have nearly the same geometrical parameters. The difference in the aspect ratios of all samples was around ± 0.1. We used EDX analysis to confirm the chemical compositions of the samples. As shown in Table 1, all the samples had the same stoichiometry 2:1:1. A higher amount of Si compared to Mn and Fe was observed in Ni_2FeSi GCMWs, Co_2FeSi MWs, and Co_2MnSi MWs due to the additional signal of Si coming from the covering glass layer.
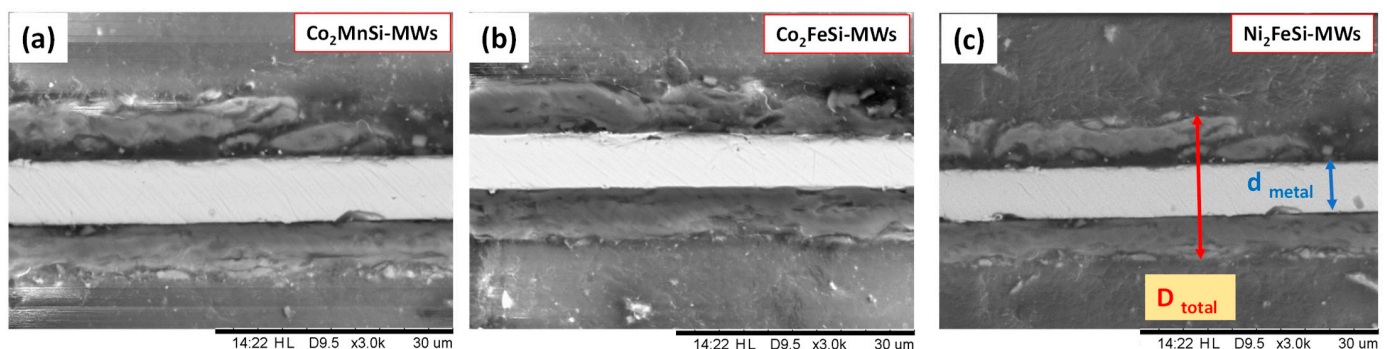

Figure 1. SEM images of (**a**) Co_2MnSi GCMWs, (**b**) Co_2FeSi GCMWs, and Ni_2FeSi GCMWs (**c**) illustrate the metallic nuclei, the coating layer, and the geometrical parameters.

Figure 2 illustrates the microstructure investigation of Ni_2FeSi, Co_2FeSi, and Co_2MnSi MWs measured by XRD at room temperature. The pattern starts from $2\Theta = 23.8°$ to exclude the amorphous halo that comes from the covering glass layers. As shown in Figure 2, all the samples showed a crystalline structure with main peaks at $2\Theta = 46.3°$. Although the samples had the same geometrical parameters, changes in the microstructure were

observed. The Ni_2FeSi and Co_2MnSi MWs shared two peaks at $2\Theta = 68.6°$ and $2\Theta = 85.1°$ with (400) and (420) reflections, respectively. Due to the absence of a (111) reflection in the Ni_2FeSi MWs, the BCC single-phase microstructure with B2 type, i.e., (disordered) is supposed. Meanwhile, a well-defined FCC single phase with $L2_1$ ordered type was found for the Co_2MnSi MWs. However, the two superlattice diffraction (111) and (200) peaks were significantly weaker compared to those for other elements belonging to the same period of the periodic table [48]. The intensities of these peaks may, therefore, be essentially undetectable if the majority or all the elements in the presented alloys belong to the same period in the elemental periodic table. For Co_2FeSi MWs, the existence of two peaks only at $2\Theta = 46.3°$ and $2\Theta = 85.1°$, corresponding with (220) and (420) reflections, fit very well with the FCC single phase with A2 type, i.e., disordered.

From detailed analysis of the XRD pattern of the Ni_2FeSi, Co_2FeSi, and Co_2MnSi MW samples, we found that the lowest lattice parameters were detected for Co_2FeSi MWs, where a = 2.81Å. The cell parameters for Ni_2FeSi and Co_2MnSi MWs were very similar, where a = 5.78 Å and 5.71 Å, respectively. However, although the samples had the same space group, i.e., $Im\overline{3}m$ (BCC) type, the crystallite size was different as illustrated in Table 2. The Co_2FeSi and Co_2MnSi glass-coated microwires had a roughly similar crystallite size ($\approx$ 37 nm), while for Ni_2FeSi MWs, it reduced to $\approx$ 21 nm. The values for crystallite size and the degree of microstructure order have a strong effect on the magnetic behavior of the samples. Thus, the diffraction peak at $2\Theta = 46.3°$ for Ni_2FeSi GCMWs appeared broader than those for the other samples.
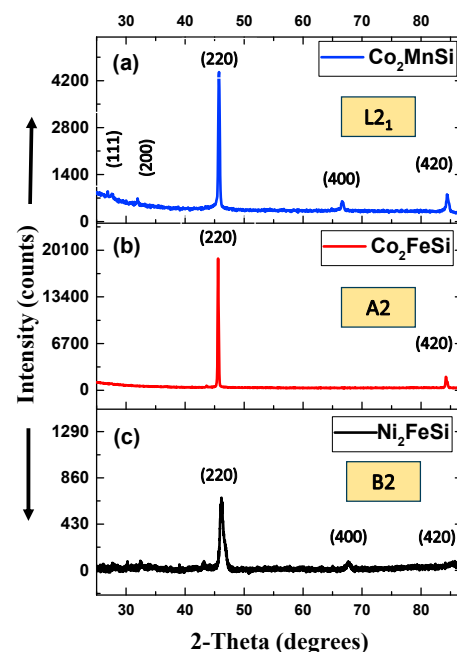

Figure 2. X-ray diffraction pattern of as-prepared Ni_2FeSi (**c**), Co_2FeSi (**b**), and Co_2MnSi (**a**) glass-coated microwires at room temperature.

Table 2. Crystallographic information of as-prepared Ni_2FeSi, Co_2FeSi, and Co_2MnSi glass-coated microwires with fixed aspect ratio.

Sample	Crystallite Size (nm)	Space Group	Cell Parameters (a (Å))	Structural Designation
Ni_2FeSi	21.3 ± 0.3	$Fm\overline{3}m$ (BCC)	5.78	B2 (disordered)
Co_2FeSi	37.3 ± 0.5	$Im\overline{3}m$ (BCC)	2.81	A2 (disordered)
Co_2MnSi	36.92 ± 0.5	$Fm\overline{3}m$ (FCC)	5.71	$L2_1$ (ordered)

3.2. Magnetic Characterization

3.2.1. Room-Temperature Magnetic Properties

To check the magnetic behavior of the Ni_2FeSi, Co_2FeSi, and Co_2MnSi MWs at room temperature, we performed the magnetic measurements in two directions, axial, i.e., parallel to the metallic nuclei axis, and out-of-plane, i.e., perpendicular to the wire axis by using a PPMS magnetometer. The out-of-plane loops appeared linear with a vanishing coercivity and a reduced remanence, i.e., H_c and $M_r \approx$ zero (not shown). The vanishing out-of-plane H_c and M_r indicate that all the magnetization lies in the in-plane (axial) direction and the out-of-plane direction is the hard magnetization axis for all the MW samples.

Figure 3 shows the M-H loops of the Ni_2FeSi, Co_2FeSi, and Co_2MnSi MWs at room temperature with an applied magnetic field parallel to the microwire axis, i.e., the axial direction. For Co_2MnSi MWs, it appears that the easy magnetization axis is not perfectly axial and is possibly tilted at an angle, away from the wire axis. Unfortunately, we do not have a way to measure the angular magnetic behavior to accurately determine the magnetic anisotropy of the sample. Ni_2FeSi MWs showed hard magnetic behavior with a coercivity of 138 Oe, which was 16 times higher than that of the Co_2MnSi MWs and 3 times higher than that of the Co_2FeSi MWs (see Table 3). The increase in the coercivity and the in-plane anisotropy field of Ni_2FeSi MWs must be attributed to their different microstructure. Surprisingly, the smallest value for crystallite size was observed for the Ni_2FeSi sample. Therefore, the high coercivity of the Ni_2FeSi sample may be associated with its disordered microstructure of B2 type, which strongly affects the magnetization reversal process, the domain structure, and its movement. In addition, the magnetocrystalline anisotropy plays an important role in the overall magnetic behavior. Thus, the enhanced coercivity detected in Ni_2FeSi MWs and the high reduced remanent magnetization of Co_2FeSi MWs suggest a scenario in which the crystalline texture affects the magnetic anisotropy. In particular, the easy magnetization axis can be aligned along the (220) and (420) reflections. However, although the Co_2MnSi MW sample showed a well-defined ordered structure with $L2_1$ type, the low reduced remanence and coercivity observed in the Co_2MnSi MW sample can be due to the mismatching between the magnetocrystalline anisotropy and the crystalline structure. As demonstrated in our previous research, the magnetic anisotropy behavior of Heusler-based glass-coated microwires is primarily influenced by two main factors: uniaxial magnetic anisotropy and cubic magnetocrystalline anisotropy [14,17]. It has been reported elsewhere [18–21,30] that the ρ-ratio is directly related to the strength of internal stresses. Therefore, it is expected, that the ρ-ratio affects the relative content of the crystalline phase and correlates with modifications in the magnetic properties. Specifically, cubic magnetocrystalline anisotropy emerges as the predominant factor governing magnetic anisotropy. Regrettably, at present, experimental measurement of this type of anisotropy remains unfeasible. However, the presence of a roughly squared hysteresis loop strongly indicates its significant impact on the magnetic properties of the Ni_2FeSi and Co_2FeSi MW samples.

Table 3. The coercivity (H_c), reduced remanence (M_r), and in-plane anisotropy field (H_k) of as-prepared Ni_2FeSi, Co_2FeSi, and Co_2MnSi glass-coated microwires with a fixed aspect ratio measured at room temperature.

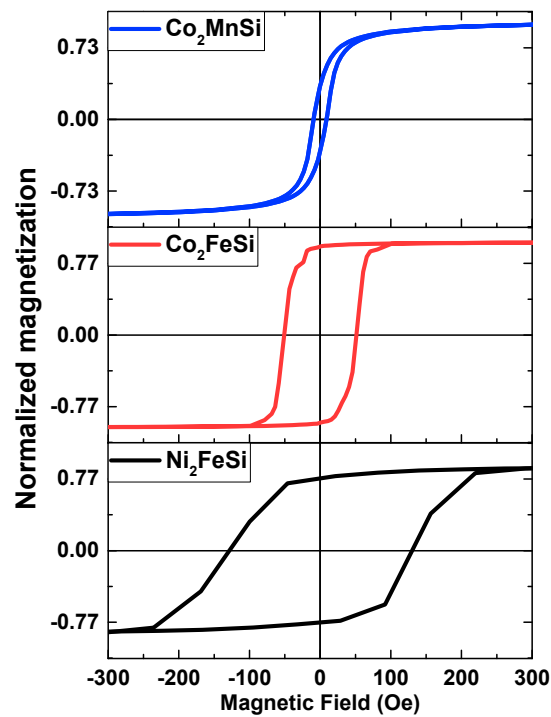| Sample	H_c (Oe)	M_r	H_k (Oe)
Ni_2FeSi	138 ± 0.5	0.82 ± 0.01	350 ± 0.5
Co_2FeSi	45 ± 0.5	0.92 ± 0.01	88 ± 0.5
Co_2MnSi	7 ± 0.5	0.22 ± 0.01	45 ± 2

Figure 3. Hysteresis loops at room temperature of as-prepared Ni_2FeSi, Co_2FeSi, and Co_2MnSi glass-coated microwires with fixed geometric parameters.

3.2.2. Temperature Dependence of Magnetic Properties

It is worth noting that the temperature stability of ferromagnetic materials is a crucial characteristic for their possible applications in spintronic and sensing devices. Hence, we investigated the magnetic behavior of the Ni_2FeSi, Co_2FeSi, and Co_2MnSi MWs with a fixed ρ-ratio for a wide range of measurement temperatures, 5–400 K. The shape of the loops follows the same trend observed at room temperature: non-squared for the Co_2MnSi MWs and quite squared for the Ni_2FeSi and Co_2FeSi MW samples. In Figures 4 and 5, the M-H loops and the evolution of H_c and M_r with the temperature are shown. This behavior can be explained by considering that, for the Ni_2FeSi and Co_2FeSi MW samples, cubic magnetocrystalline anisotropy prevails up to 400 K.
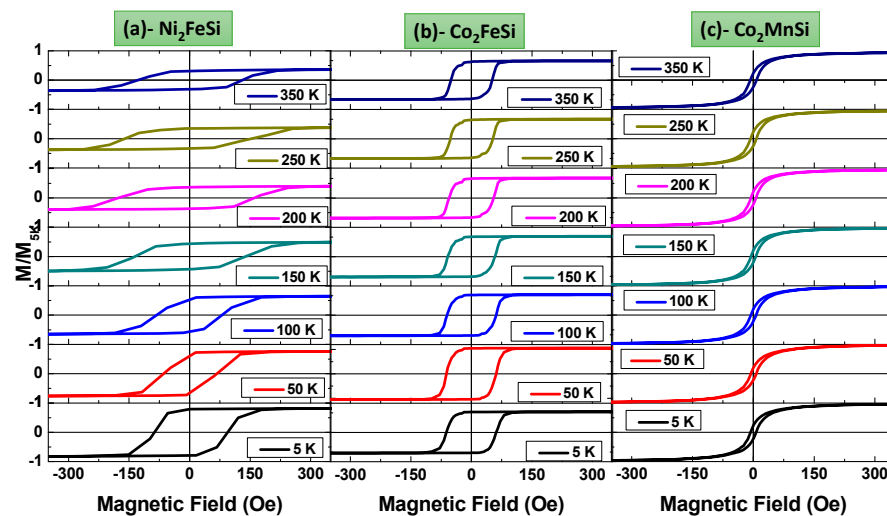

Figure 4. Hysteresis loops at different temperatures of as-prepared Ni_2FeSi, Co_2FeSi, and Co_2MnSi glass-coated microwires with fixed aspect ratio. All loops were measured at a temperature range from 350 K to 5 K.
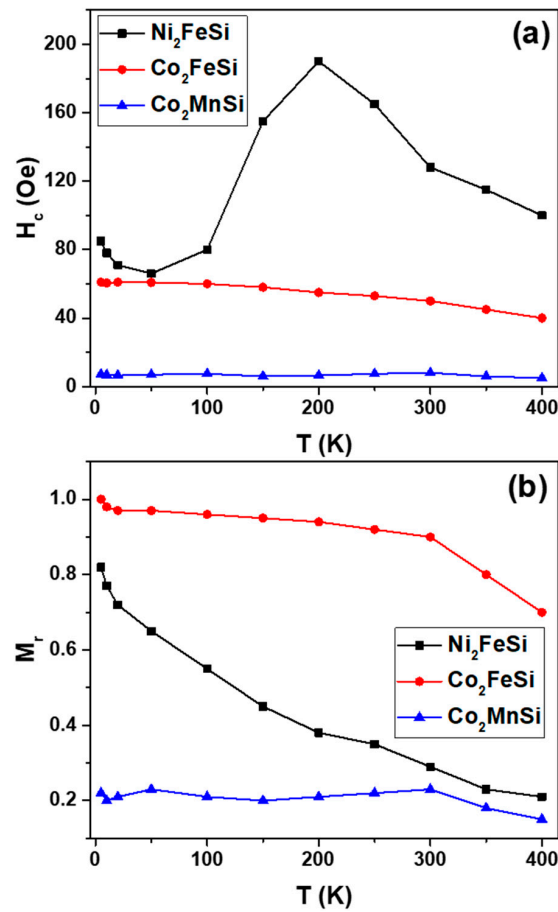
Figure 5. Temperature dependence of the coercivity (**a**) and normalized remanence (**b**) of as-prepared Ni_2FeSi, Co_2FeSi, and Co_2MnSi glass-coated microwires with fixed aspect ratio. (Lines for eye guide).

By analyzing the M-H loops measured at the temperature range 5–350 K for Ni_2FeSi, Co_2FeSi, and Co_2MnSi MWs with a fixed ρ-ratio, an interesting magnetic behavior was observed for the temperature dependence of H_c in Ni_2FeSi MWs. First, the Ni_2FeSi MWs showed the highest coercivity value at all temperature ranges compared to the Co_2-based glass-coated samples with the same aspect ratio. In addition, the H_c temperature dependence did not show uniform behavior; two flipped points at T = 200 K and 50 K were observed. At these points, the tendency of H_c dramatically changed with temperature (see Figure 4a). Meanwhile, the temperature dependence of H_c for Co_2FeSi and Co_2MnSi MWs showed quite a stable tendency with temperature. The improved coercivity stability observed in Co_2MnSi MWs is strongly related to the high-ordered microstructure with $L2_1$ type (see Figure 1). However, both the Ni_2FeSi and the Co_2FeSi MWs had a disordered microstructure with B2 type and A2 type, respectively. The Co_2FeSi MWs showed higher coercivity thermal stability due to their A2 type microstructure, which shows higher energy stability compared to the B2 type [49–51]. Thus, the Co_2FeSi MWs' Hc vs. T appeared more stable compared to that of Ni_2FeSi MWs. Additionally, the M_r vs. T tendency displayed regular ferromagnetic behavior with temperature, where a monotonic increase in M_r was observed with decreasing T (see Figure 4b). Both Ni_2FeSi and Co_2FeSi MWs had higher M_r values for the entire range of measuring temperatures compared to Co_2MnSi MWs. The higher values of M_r for Ni_2FeSi and Co_2FeSi MWs suggest a dominant cubic magnetocrystalline anisotropy at a wide range of measuring temperatures.

Figure 6 shows the complete thermomagnetic behavior of Ni_2FeSi, Co_2FeSi, and Co_2MnSi MWs with a fixed ρ-ratio. We studied the FC and FH temperature dependence of magnetization to check any possible phase transition. Thus, the measurements were performed at a low magnetic field of 50 Oe. The Ni_2FeSi MWs showed regular ferromagnetic

behavior wherein the FC and FH curves increased on decreasing the temperature from 400 to 5 K. For Co_2FeSi and Co_2MnSi MWs, the FC and FH magnetization curves showed non-homogonous behavior, besides an irreversible magnetic behavior that occurred at T = 125 K. Among the factors that affect irreversible behavior of the magnetization versus temperature are the induced martensitic transition and the change in the internal stresses associated with the glass-coating layer with temperature. As illustrated in Figure 6, the FC and FH magnetizations curves showed a perfect matching and monotonic increase on decreasing the temperature from 400 to 5 K in the Ni_2FeSi sample (see Figure 6a). Accordingly, we can assume that the internal stress induced by the covering glass-layer during the fabrication process had a stable and uniform effect on the magnetic properties of the Ni_2FeSi sample. Meanwhile, for Co_2FeSi and Co_2MnSi MWs, the internal stress did not show a uniform effect at all temperature ranges; from 400 to 300 K, the FC and FH had a good matching behavior, but on decreasing the temperature below 300 K, mismatching started to appear. Due to the disordered microstructure nature of the Co_2FeSi MWs, the FC and FH did not have a smooth behavior with temperature unlike the Co_2MnSi MWs.

The current results reveal that the influence of the internal stress induced by the glass coating layer is very sensitive to the chemical composition and the microstructure ordering of X_2YZ-based glass-coated microwires. As a result, different magnetic and structural responses were observed in glass-coated microwires with different metallic nucleus chemical compositions. In our previous work, we illustrated how the internal stress is strongly related to the geometric dimensions and showed the importance of the external applied field, the annealing temperature/time condition, and the microstructure ordering of the host metallic alloys.
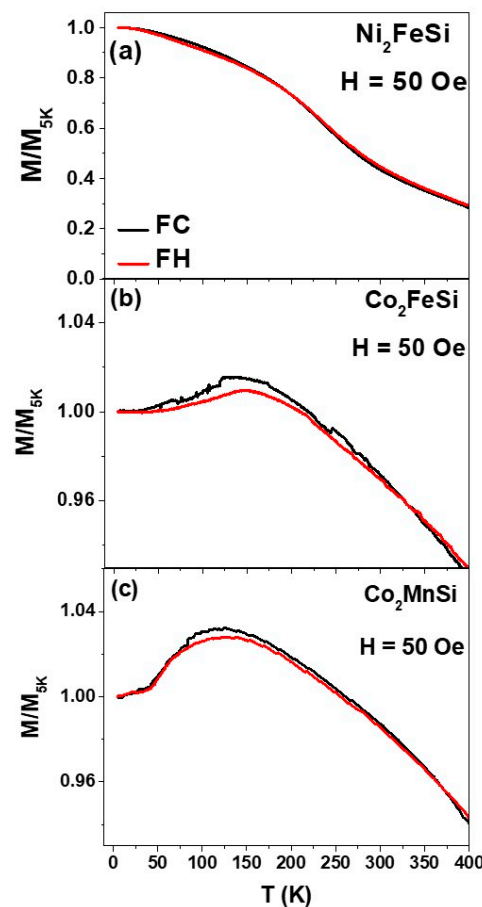

Figure 6. Temperature dependence of the measured magnetization of as-prepared (**a**) Ni_2FeSi, (**b**) Co_2FeSi, and (**c**) Co_2MnSi glass-coated microwires with a fixed aspect ratio and an applied external magnetic field of 50 Oe.

4. Discussion

During the preparation process of ferromagnetic glass-coated microwires, complex internal stresses of a tensor character are induced, determining their magnetic/structural properties. The difference between the thermal expansion coefficients of the metallic alloy and glass, quenching internal stresses associated with the fast solidification of the metallic alloy, and drawing stresses are the three main sources of internal stresses, σ_i, in glass-coated microwires [18–21,30]. It is generally accepted that the largest are the internal stresses arising due to the difference in the thermal expansion coefficients of the glass coating and the metallic alloy [18–21,30,43–45]. Moreover, all the internal stress components are affected by the geometrical parameter ($\rho = d_{metal}/D_{total}$). Thus, we can simply estimate σ_i as follows [24,45]:

$$\sigma_\varphi = \sigma_r = P = \varepsilon Ek\Delta/(k/3+1)\Delta + 4/3 \tag{1}$$

$$\sigma_z = P(k+1)\Delta + 2/(k\Delta + 1) \tag{2}$$

where σ_z, σ_φ, and σ_r are axial, circular, and radial stresses, respectively; $\Delta = (1 - \rho^2)/\rho^2$; $k = E_g/E_m$, E_m, E_g—Young modulus of metallic nucleus and glass, respectively; $\varepsilon = (\alpha_m - \alpha_g)(T_m - T_{room})$, α_m, α_g are thermal expansion coefficients of metallic nucleus and glass, respectively, and T_m and T_{room} are the melting temperature and the room temperature, respectively. Therefore, a correlation is usually assumed between the magnitude of internal stresses and the geometric ratio ρ [45]. However, the metallic alloy composition is also relevant when using the Taylor–Ulitovsky method [24]. Thus, the alloy melting temperature, good wetting with glass, and the diffusion coefficients can substantially affect the microstructure and, hence, the magnetic properties of GCMWs [24]. The origin of the quenching internal stress is related to the solidification of the metallic alloy from the surface toward the wire axis [24,44]. Due to the different conditions for the solidification process for Co_2FeSi, Co_2MnSi, and Ni_2FeSi GCMWs, the microstructure and even the magnitude of the quenching internal stress can be different. The same scenario is expected for the stresses induced by the difference in thermal expansion coefficients of the metallic alloy and glass and the drawing stresses, which are dependent on the metallic alloy as well. The previous investigations to evaluate such internal stress components took into consideration the successive concentric cylindrical shells solidifying consecutively, starting from the outside, due to the temperature gradient at the glass transition temperature [19,24,44,45].

The introduction of differences in ε, k, T_m, and T_{room} while keeping the geometrical parameters fixed is one of the routes to control the magnetic behavior of the different metallic nuclei of X_2YZ-based glass-coated microwires.

5. Conclusions

In summary, we succeeded in preparing X_2YZ-based glass-coated microwires with the same aspect ratio. In such X_2YZ-based glass-coated microwires, we studied the effect of different chemical compositions of magnetic materials, i.e., metallic nuclei, on the internal stress. Also, we illustrated three main sources of the internal stresses that control the magneto-structural behavior of the X_2YZ-based glass-coated microwires (thermal expansion coefficients of the metallic alloy and glass, quenching internal stresses, and drawing stresses). By fixing the internal stress, which mainly depends on the geometrical parameters, a notable variation in the magnetic and structural properties was observed. In the microstructure investigation, for Co_2FeSi and Ni_2FeSi MWs, the microstructure features were found to be disordered, varying between the A2 type and the B2 type, respectively. Meanwhile, a well-defined, ordered $L2_1$ type microstructure was observed for Co_2MnSi-based glass-coated microwires. The variation in the microstructure has a strong effect on the magnetic behavior of the samples, resulting in a notable change in the H_c, H_k, M_r, FC, and FH tendency with temperature and magnetic field. There were also differences in the quenching internal stress and the internal stresses originated by different thermal expansion coefficients of the metallic alloy and glass, i.e., changing the metallic nucleus composition leads to changes in the magnetic and structural properties. The high thermal

stability of coercivity observed in Co_2MnSi- and Co_2FeSi-based glass-coated microwires makes them promising candidates for different industrial applications.

References

1. Heusler, F. Verhandlungen Dtsch. *Phys. Ges.* **1903**, *5*, 219.
2. Elphick, K.; Frost, W.; Samiepour, M.; Kubota, T.; Takanashi, K.; Sukegawa, H.; Mitani, S.; Hirohata, A. Heusler Alloys for Spintronic Devices: Review on Recent Development and Future Perspectives. *Sci. Technol. Adv. Mate.* **2021**, *22*, 235–271. [CrossRef]
3. Bai, Z.; Shen, L.E.I.; Han, G.; Feng, Y.P. Data Storage: Review of Heusler Compounds. *Spin* **2012**, *2*, 1230006. [CrossRef]
4. Chumak, O.M.; Pacewicz, A.; Lynnyk, A.; Salski, B.; Yamamoto, T.; Seki, T.; Domagala, J.Z.; Głowiński, H.; Takanashi, K.; Baczewski, L.T.; et al. Magnetoelastic Interactions and Magnetic Damping in $Co_2Fe_{0.4}Mn_{0.6}Si$ and $Co_2FeGa_{0.5}Ge_{0.5}$ Heusler Alloys Thin Films for Spintronic Applications. *Sci. Rep.* **2021**, *11*, 7608. [CrossRef]
5. Li, P.; Koo, J.; Ning, W.; Li, J.; Miao, L.; Min, L.; Zhu, Y.; Wang, Y.; Alem, N.; Liu, C.X.; et al. Giant room temperature anomalous Hall effect and tunable topology in a ferromagnetic topological semimetal Co_2MnAl. *Nat. Commun.* **2020**, *11*, 3476. [CrossRef] [PubMed]
6. Gutfleisch, O.; Willard, M.A.; Bruck, E.; Chen, C.H.; Sankar, S.G.; Liu, J.P. Magnetic Materials and Devices for the 21st Century: Stronger, Lighter, and More Energy Efficient. *Adv. Mater.* **2011**, *23*, 821–842. [CrossRef]
7. Franco, V.; Blázquez, J.S.; Ipus, J.J.; Law, J.Y.; Moreno-Ramírez, L.M.; Conde, A. Magnetocaloric effect: From materials research to refrigeration devices. *Prog. Mater. Sci.* **2018**, *93*, 112–232. [CrossRef]
8. Chatterjee, S.; Chatterjee, S.; Giri, S.; Majumdar, S. Transport properties of Heusler compounds and alloys. *J. Phys. Condens. Matter* **2022**, *34*, 013001. [CrossRef] [PubMed]
9. Silber, R.; Kral, D.; Stejskal, O.; Kubota, T.; Ando, Y.; Pistora, J.; Veis, M.; Hamrle, J.; Kuschel, T. Scaling of quadratic and linear magneto-optic Kerr effect spectra with $L2_1$ ordering of Co_2MnSi Heusler compound. *Appl. Phys. Lett.* **2020**, *116*, 262401. [CrossRef]
10. Tavares, S.; Yang, K.; Meyers, M.A. Heusler alloys: Past, properties, new alloys, and prospects. *Prog. Mater. Sci.* **2023**, *132*, 101017. [CrossRef]
11. Balke, B.; Wurmehl, S.; Fecher, G.H.; Felser, C.; Kübler, J. Rational Design of New Materials for Spintronics: Co_2FeZ (Z=Al, Ga, Si, Ge). *Sci. Technol. Adv. Mater.* **2008**, *9*, 014102. [CrossRef]
12. Jourdan, M.; Minár, J.; Braun, J.; Kronenberg, A.; Chadov, S.; Balke, B.; Gloskovskii, A.; Kolbe, M.; Elmers, H.J.; Schönhense, G.; et al. Direct observation of half-metallicity in the Heusler compound Co_2MnSi. *Nat. Commun.* **2014**, *5*, 3974. [CrossRef]
13. Životský, O.; Skotnicová, K.; Čegan, T.; Juřica, J.; Gembalová, L.; Zažímal, F.; Szurman, I. Structural and Magnetic Properties of Inverse-Heusler Mn_2FeSi Alloy Powder Prepared by Ball Milling. *Materials* **2022**, *15*, 697. [CrossRef] [PubMed]
14. Salaheldeen, M.; Garcia, A.; Corte-Leon, P.; Ipatov, M.; Zhukova, V.; Zhukov, A. Unveiling the Effect of Annealing on Magnetic Properties of Nanocrystalline Half-Metallic Heusler Co_2FeSi Alloy Glass-Coated Microwires. *J. Mater. Res. Technol.* **2022**, *20*, 4161–4172. [CrossRef]

15. Khovaylo, V.V.; Rodionova, V.V.; Shevyrtalov, S.N.; Novosad, V. Magnetocaloric Effect in "Reduced" Dimensions: Thin Films, Ribbons, and Microwires of Heusler Alloys and Related Compounds. *Phys. Status Solidi* **2014**, *251*, 2104–2113. [CrossRef]

16. Herzer, G. Amorphous and Nanocrystalline Materials. In *Encyclopedia of Materials: Science and Technology*; Elsevier: Amsterdam, The Netherlands, 2001; pp. 149–156. [CrossRef]

17. Salaheldeen, M.; Garcia-Gomez, A.; Corte-León, P.; Gonzalez, A.; Ipatov, M.; Zhukova, V.; Gonzalez, J.M.; López Antón, R.; Zhukov, A. Manipulation of Magnetic and Structure Properties of Ni_2FeSi Glass-Coated Microwires by Annealing. *J. Alloys Compd.* **2023**, *942*, 169026. [CrossRef]

18. Antonov, A.S.; Borisov, V.T.; Borisov, O.V.; Prokoshin, A.F.; Usov, N.A. Residual quenching stresses in glass-coated amorphous ferromagnetic microwires. *J. Phys. D Appl. Phys.* **2000**, *33*, 1161–1168. [CrossRef]

19. Zhukova, V.; Cobeño, A.F.; Zhukov, A.; de Arellano Lopez, A.R.; López-Pombero, S.; Blanco, J.M.; Larin, V.; Gonzalez, J. Correlation between magnetic and mechanical properties of devitrified glass-coated $Fe_{71.8}Cu_1Nb_{3.1}Si_{15}B_{9.1}$ microwires. *J. Magn. Magn. Mater.* **2002**, *249*, 79–84. [CrossRef]

20. Wang, C.; Cao, G.; Liu, J.; Zhang, Y.; Liu, R.; Wang, F.; Zhang, M.; Wang, L.; Zhang, B. Direct Current Annealing Modulated Ordered Structure to Optimize Tensile Mechanical Properties of Co-Based Amorphous Metallic Microwires. *Metals* **2022**, *12*, 1427. [CrossRef]

21. Chiriac, H.; Óvári, T.A.; Pop, G. Internal stress distribution in glass-covered amorphous magnetic wires. *Phys. Rev. B* **1995**, *52*, 10104–10113. [CrossRef]

22. Ulitovsky, A.V.; Maianski, I.M.; Avramenco, A.I. 1960 Method of Continuous Casting of Glass Coated Microwire. USSR Patent 128427, 6 May 2015.

23. Salaheldeen, M.; Wederni, A.; Ipatov, M.; Zhukova, V.; Zhukov, A. Carbon-Doped Co_2MnSi Heusler Alloy Microwires with Improved Thermal Characteristics of Magnetization for Multifunctional Applications. *Materials* **2023**, *16*, 5333. [CrossRef] [PubMed]

24. Salaheldeen, M.; Garcia-Gomez, A.; Corte-Leon, P.; Ipatov, M.; Zhukova, V.; Gonzalez, J.; Zhukov, A. Anomalous Magnetic Behavior in Half-Metallic Heusler Co_2FeSi Alloy Glass-Coated Microwires with High Curie Temperature. *J. Alloys Compd.* **2022**, *923*, 166379. [CrossRef]

25. Nematov, M.G.; Baraban, I.; Yudanov, N.A.; Rodionova, V.; Qin, F.X.; Peng, H.X.; Panina, L.V. Evolution of the magnetic anisotropy and magnetostriction in Co-based amorphous alloys microwires due to current annealing and stress-sensory applications. *J. Alloys Compd.* **2020**, *837*, 155584. [CrossRef]

26. Salaheldeen, M.; Wederni, A.; Ipatov, M.; Zhukova, V.; Lopez Anton, R.; Zhukov, A. Enhancing the Squareness and Bi-Phase Magnetic Switching of Co_2FeSi Microwires for Sensing Application. *Sensors* **2023**, *23*, 5109. [CrossRef] [PubMed]

27. Chiriac, H.; Lupu, N.; Stoian, G.; Ababei, G.; Corodeanu, S.; Óvári, T.A. Ultrathin Nanocrystalline Magnetic Wires. *Crystals* **2017**, *7*, 48. [CrossRef]

28. Salaheldeen, M.; Ipatov, M.; Zhukova, V.; García-Gomez, A.; Gonzalez, J.; Zhukov, A. Preparation and magnetic properties of Co_2-based Heusler alloy glass-coated microwires with high Curie temperature. *AIP Adv.* **2023**, *13*, 025325. [CrossRef]

29. Salaheldeen, M.; Wederni, A.; Ipatov, M.; Gonzalez, J.; Zhukova, V.; Zhukov, A. Elucidation of the Strong Effect of the Annealing and the Magnetic Field on the Magnetic Properties of Ni_2-Based Heusler Microwires. *Crystals* **2022**, *12*, 1755. [CrossRef]

30. Torcunov, A.V.; Baranov, S.A.; Larin, V.S. The internal stresses dependence of the magnetic properties of cast amorphous microwires covered with glass insulation. *J. Magn. Magn. Mater.* **1999**, *196–197*, 835–836. [CrossRef]

31. Kozejova, D.; Fecova, L.; Klein, P.; Sabol, R.; Hudak, R.; Sulla, I.; Mudronova, D.; Galik, J.; Varga, R. Biomedical Applications of Glass-Coated Microwires. *J. Magn. Magn. Mater.* **2019**, *470*, 2–5. [CrossRef]

32. Grabco, D.; Dyntu, M.; Meglei, D.; Shikimaka, O. Microstructure and Strength Properties of Germanium Microwires for Biomedical Devices. In *Nanostructured Materials and Coatings for Biomedical and Sensor Applications*; Gogotsi, Y.G., Uvarova, I.V., Eds.; NATO Science Series; Springer: Dordrecht, The Netherlands, 2003; Volume 102. [CrossRef]

33. Mitxelena-Iribarren, O.; Campisi, J.; de Apellániz, I.M.; Lizarbe-Sancha, S.; Arana, S.; Zhukova, V.; Mujika, M.; Zhukov, A. Glass-coated ferromagnetic microwire-induced magnetic hyperthermia for in vitro cancer cell treatment. *Mater. Sci. Eng. C* **2020**, *106*, 110261. [CrossRef]

34. Gomez-Polo, C.; Perez-Landazabal, J.I.; Recarte, V.; Sanchez-Alarcos, V.; Badini-Confalonieri, G.; Vazquez, M. Ni-Mn-Ga ferromagnetic shape memory wires. *J. Appl. Phys.* **2010**, *107*, 123908. [CrossRef]

35. Salaheldeen, M.; Wederni, A.; Ipatov, M.; Zhukova, V.; Zhukov, A. Preparation and Magneto-Structural Investigation of High-Ordered ($L2_1$ Structure) Co_2MnGe Microwires. *Processes* **2023**, *11*, 1138. [CrossRef]

36. Salaheldeen, M.; Talaat, A.; Ipatov, M.; Zhukova, V.; Zhukov, A. Preparation and Magneto-Structural Investigation of Nanocrystalline CoMn-Based Heusler Alloy Glass-Coated Microwires. *Processes* **2022**, *10*, 2248. [CrossRef]

37. Hennel, M.; Varga, M.; Frolova, L.; Nalevanko, S.; Ibarra-Gaytán, P.; Vidyasagar, R.; Sarkar, P.; Dzubinska, A.; Galdun, L.; Ryba, T.; et al. Heusler-Based Cylindrical Micro- and Nanowires. *Phys. Status Solidi A* **2022**, *219*, 2100657. [CrossRef]

38. Zhukov, A.; Ipatov, M.; del Val, J.J.; Zhukova, V.; Chernenko, V.A. Magnetic and structural properties of glass-coated Heusler-type microwires exhibiting martensitic transformation. *Sci. Rep.* **2018**, *8*, 621. [CrossRef] [PubMed]

39. Salaheldeen, M.; Ipatov, M.; Corte-Leon, P.; Zhukova, V.; Zhukov, A. Effect of Annealing on the Magnetic Properties of Co_2MnSi-Based Heusler Alloy Glass-Coated Microwires. *Metals* **2023**, *13*, 412. [CrossRef]

40. Hennel, M.; Galdun, L.; Džubinská, A.; Reiffers, M.; Varga, R. High efficiency direct magnetocaloric effect in Heusler Ni_2MnGa microwire at low magnetic fields. *J. Alloys Compd.* **2023**, *960*, 170621. [CrossRef]

41. Zhukov, A.; Garcia, C.; Ilyn, M.; Varga, R.; del Val, J.J.; Granovsky, A.; Rodionova, V.; Ipatov, M.; Zhukova, V. Magnetic and transport properties of granular and Heusler-type glass-coated microwires. *J. Magn. Magn. Mater.* **2012**, *324*, 3558–3562. [CrossRef]

42. Zhukova, V.; Aliev, A.M.; Varga, R.; Aronin, A.; Abrosimova, G.; Kiselev, A.; Zhukov, A. Magnetic Properties and MCE in Heusler-Type Glass-Coated Microwires. *J. Supercond. Nov. Magn.* **2013**, *26*, 1415–1419. [CrossRef]

43. Baranov, S.A.; Larin, V.S.; Torcunov, A.V. Technology, Preparation and Properties of the Cast Glass-Coated Magnetic Microwires. *Crystals* **2017**, *7*, 136. [CrossRef]

44. Chiriac, H.; Ovari, T.-A. Amorphous glass-covered magnetic wires: Preparation, properties, applications. *Prog. Mater. Sci.* **1996**, *40*, 333–407. [CrossRef]

45. Zhukova, V.; Blanco, J.M.; Ipatov, M.; Zhukov, A. Magnetoelastic contribution in domain wall dynamics of amorphous microwires. *Physica B* **2012**, *407*, 1450–1454. [CrossRef]

46. Klein, P.; Varga, R.; Badini-Confalonieri, G.A.; Vazquez, M. Domain Wall Dynamics in Amorphous and Nanocrystalline 492 FeCoMoB Microwires. *J. Nanosci. Nanotechnol.* **2012**, *12*, 7464–7467. [CrossRef] [PubMed]

47. Corodeanu, S.; Hlenschi, C.; Chiriac, H.; Óvári, T.-A.; Lupu, N. Comparative Study of the Magnetic Behavior of FINEMET Thin Magnetic Wires: Glass-Coated, Glass-Removed, and Cold-Drawn. *Materials* **2023**, *16*, 1340. [CrossRef] [PubMed]

48. Salaheldeen, M.; Zhukova, V.; Wederni, A.; Ipatov, M.; Zhukov, A. Magnetic Properties of Co_2MnSi-based Heusler Alloy Glass-coated Microwires. *IEEE Trans. Magn.* **2023**, *59*, 7300904. [CrossRef]

49. Ahmad, A.; Mitra, S.; Srivastava, S.K.; Das, A.K. Size-Dependent Structural and Magnetic Properties of Disordered Co_2FeAl Heusler Alloy Nanoparticles. *J. Magn. Magn. Mater.* **2019**, *474*, 599–604. [CrossRef]

50. Zhang, X.; Han, L.; Dehm, G.; Liebscher, C.H. Microstructure and Physical Properties of Dual-Phase Soft Magnetic Fe-Co-Ti-Ge Alloys. *J. Alloys Compd.* **2023**, *945*, 169282. [CrossRef]

51. Zhang, H.G.; Song, B.T.; Chen, J.; Yue, M.; Liu, E.K.; Wang, W.H.; Wu, G.H. Magnetization Variation in Fe–Cr-Ga System. *Intermetallics* **2019**, *113*, 106580. [CrossRef]